Organic Electronics 54 (2018) 167–176

Contents lists available at ScienceDirect

Organic Electronics

journal homepage: www.elsevier.com/locate/orgel

Red-light-emitting electrochemical cells based on cationic iridium complexes with phenanthroimidazole-type ancillary ligand

Jo Yeonah[a], Chozhidakath Damodharan Sunesh[a], Ramesh Kumar Chitumalla[b], Joonkyung Jang[b], Youngson Choe[a,*]

[a] Department of Polymer Science and Chemical Engineering, Pusan National University, Busan 609-735, Republic of Korea
[b] Department of Nanoenergy Engineering, Pusan National University, Busan 609-735, Republic of Korea

ARTICLE INFO

Keywords:
Phenanthroimidazole
Iridium complexes
Red emission
Self-quenching
Electroluminescent properties

ABSTRACT

Red-emitting cationic iridium complexes, namely, $[Ir(ppy)_2(Qtpi)]PF_6$ (Complex 1) and $[Ir(piq)_2(Qtpi)]PF_6$ (Complex 2) were synthesized using the ancillary ligand 2-(quinolin-2-yl)-1-(*p*-tolyl)-1*H*-phenanthro[9,10-*d*] imidazole (Qtpi) and 2-phenylpyridine (Hppy) and 1-phenylisoquinoline (Hpiq) as cyclometalating ligands. In acetonitrile solution, Complex 1 emitted orange light, centered at 614 nm, whereas Complex 2 gave rise to orange-red emission centered at 603 and a shoulder peak at 630 nm. Extended π-conjugation on the phenylpyridine ligand in Complex 2 lowered the energy-gap, leading to a red-shift the emission compared to that of Complex 1. A light-emitting electrochemical cell (LEC) fabricated with Complex 1 emitted red light with an emission peak at 618 nm and Commission Internationale de L'Eclairage (CIE) coordinates of (0.59, 0.36), respectively, with corresponding values of 692 nm and (0.56, 0.28) for Complex 2. The LEC based on Complex 1 demonstrated superior performance, with a maximum luminance and current efficiency of 808 cd m^{-2} and 0.73 cd A^{-1}, respectively.

1. Introduction

Worldwide energy consumption has continued to escalate each year, wherein about 20% of the world's energy is utilized for lighting. To achieve energy-saving in lighting, it is very important to increase the efficiency of lighting devices in a sustainable way. Light-emitting electrochemical cells (LECs) are prominent lighting devices with simple device architecture: a luminescent emitter sandwiched between two metal electrodes (i.e. a reflective cathode and transparent anode) [1–4]. LECs are solution-processed solid-state lighting devices comprising a luminescent material in an ionic environment. The mobile ions in the active layer drift towards the relevant electrodes under an external bias and accumulate at the electrode interfaces, forming electrical double layers (EDLs); these EDLs facilitate the injection of holes and electrons from the anode and cathode, respectively. Since LEC devices are insensitive to the electrode work function, air-stable electrodes such as Au, Ag, or Al are used for their fabrication. This facilitates device fabrication under ambient conditions and precludes the requirements for rigorous encapsulation. In contrast, multilayered organic light-emitting diodes (OLEDs) rely on air-sensitive charge injection layers and low-work-function electrodes and require device encapsulation, resulting in a high manufacturing cost, which hinders their widespread use in the lighting industry [5]. The above limitations of OLEDs have led to the concept of LECs as next-generation, low-cost, large-area devices for display and lighting applications that should circumvent the prevailing problems of OLEDs.

The luminescent materials used in LECs are based on either polymers (PLECs) [1] or ionic transition metal complexes (iTMCs-LECs) [6–12]. In PLECs, emissive conjugated polymers are mixed with an ion-conducting polymer and an inorganic salt to achieve ionic conductivity [1]. In the case of iTMCs-LECs, the use of an additional ion conducting material to drive the device is not a prerequisite as iTMCs are intrinsically ionic in nature. The first solid-state LECs utilizing iTMCs were reported in 1996, based on a ruthenium polypyridyl complex as the light-emitting material [13]. However, the inadequate color tuning of Ru complexes because of their low ligand-field splitting energies

Abbreviations: AFM, Atomic force microscopy; CT, charge transfer; DFT, density functional theory; EDLs, electrical double layers; EL, electroluminescence; Hppy, 2-phenylpyridine; Hpiq, 1-phenylisoquinoline; ITO, indium tin oxide; iTMCs, ionic transition metal complexes; LC, ligand-centered; ^{1}LLCT, ligand-to-ligand charge transfer; LEC, light-emitting electrochemical cell; LFSEs, ligand-field splitting energies; ^{1}MLCT, metal-to-ligand charge transfer; OLEDs, organic light-emitting diodes; PL, photoluminescence; PLQYs, photoluminescence quantum yields; PCM, polarizable continuum model; PLEC, polymer light-emitting electrochemical cell; Qtpi, 2-(quinolin-2-yl)-1-(*p*-tolyl)-1*H*-phenanthro[9,10-*d*]imidazole; rms, root-mean-square; $TBAPF_6$, tetrabutylammonium hexafluorophosphate; TGA, thermogravimetric analysis; TDDFT, time-dependent density functional theory

* Corresponding author.
E-mail address: choe@pusan.ac.kr (Y. Choe).

https://doi.org/10.1016/j.orgel.2017.12.035
Received 21 October 2017; Received in revised form 14 December 2017; Accepted 22 December 2017
Available online 27 December 2017

(LFSEs) limits their utility in display and lighting technologies that demand wider color tunability. In order to tune the emission colors, LECs based on the cationic iridium complex, $[Ir(ppy)_2(dtb\text{-}bpy)]PF_6$ were first fabricated by Slinker et al. in 2004; these LECs emit in the yellow region of the visible spectrum with a peak brightness and power efficiency of 300 cdm^{-2} and 10 lm W^{-1}, respectively at 3 V [2]. Compared to other reported iTMCs, the cyclometalated Ir(III) complexes show outstanding properties due to their high metal oxidation states and the presence of strong-field anionic cyclometalating ligands (CˆN) producing large LFSEs [14–16]. In addition, the strong spin–orbit coupling of iridium complexes enables efficient intersystem crossing between the triplet and singlet states, resulting in theoretical efficiencies of 100%. Moreover, color tuning of iridium complexes from blue to red can be achieved via chemical modification of the organic ligands. The aforementioned characteristics of iridium complexes can lead to high emission quantum yields, short excited-state lifetimes, and remarkable color tunability with excellent thermal and photochemical stabilities.

A large number of iridium complexes have been reported for LEC applications; however, red-emitting devices are scarce because most of the developed devices emit in the orange or orange-red spectral region [17,18]. However, red-emitting devices are crucial for the fabrication of white-light devices through additive color mixing, as well as for signaling applications [19–21]. Red-emitting iridium complexes are obtained via structural modification of both cyclometalating (CˆN) and ancillary (NˆN) ligands of the archetypal iridium complex, $[Ir(CˆN)_2(NˆN)]PF_6$. The addition of electron-donating groups to the phenyl ring of the CˆN ligand or incorporation of electron-withdrawing substituents on the NˆN ligand are potential strategies for shifting the emission to the red region [22,23]. The former causes destabilization of the highest occupied molecular orbital (HOMO) and the latter leads to stabilization of the lowest unoccupied molecular orbital (LUMO), thereby resulting in a narrow HOMO − LUMO energy gap. Increasing the delocalization of the π system of the CˆN and NˆN ligands also results in tuning of the iridium complex emission to the red spectral region [24,25]. In addition to the color tunability, stability of the iridium complex is also crucial for practical application. During device operation, the iridium complexes may experience severe excited-state self-quenching because the complexes are closely packed in the device architecture. The stability of iridium complexes can be enhanced by incorporating bulky substituents on ancillary ligands or by introducing π–π interactions, thereby reducing both water-induced substitution reactions and non-radiative pathways, and hence can augment both the efficiency and lifetime of the devices [6,18,26,27].

Herein, we present an account of the synthesis and characterization of two new cationic iridium complexes, namely, $[Ir(ppy)_2(Qtpi)]PF_6$ (Complex 1) and $[Ir(piq)_2(Qtpi)]PF_6$ (Complex 2) using 2-(quinolin-2-yl)-1-(*p*-tolyl)-1*H*-phemnanthro[9,10-*d*]imidazole (Qtpi) as an ancillary ligand and 2-phenylpyridine (Hppy) and 1-phenylisoquinoline (Hpiq) as cyclometalating ligands for the fabrication of efficient red-emitting devices. The ancillary ligand Qtpi was chosen due to its remarkable photophysical properties, thermal stability, and balanced charge transport ability. The cationic iridium complexes (Complexes 1 and 2), synthesized using Qtpi, show orange emission (614 nm) and orange-red emission (603 and 630 nm), respectively, in acetonitrile solution. Cyclic voltammetric measurements were performed on both complexes and the results are supported by density functional theory (DFT) calculations. Complexes 1 and 2 were incorporated into LECs; these devices display red-shifted electroluminescence (EL) spectra compared to the PL spectra in solution. The red-emitting LECs based on Complex 1 and Complex 2 show peak current efficiencies of 0.73 and 0.20 cd A^{-1}, respectively. Moreover, the complexes show high stability with increasing voltage, which may be attributed to decreased intermolecular interaction and luminescence self-quenching due to the presence of the *N*-aryl group attached to the imidazole moiety of Qtpi. Based on the results, the use of phenanthroimidazole in iridium complexes is anticipated to significantly contribute to the advancement of display and lighting technologies.

2. Materials and methods

2.1. Materials

All chemicals and reagents from commercial suppliers were used without further purification, including iridium(III) chloride hydrate (99.9%, Alfa Aesar), quinoline-2-carboxaldehyde (97%, Alfa Aesar), *p*-toluidine (> 99%, TCI), 9,10-phenanthrenequinone (95%, Sigma Aldrich), and ammonium acetate (≥98%, Sigma Aldrich). ^1H and ^{13}C NMR spectra of the complexes in CD_2Cl_2 were acquired on a Unity-Inova 500 MHz FT-NMR spectrometer with tetramethylsilane (TMS) as an internal standard (the *J* values are given in Hz). Elemental analyses were performed on an Elementar Vario EL CHN elemental analyzer. Electrospray ionization mass spectrometric (ESI-MS) analyses were conducted with an Agilent Q-TOF 6530 MS/MS system. The UV–visible absorption spectra of the complexes in acetonitrile solutions (10^{-5} M) were recorded at room temperature using an Agilent 8453 spectrophotometer. Photoluminescence (PL) emission spectra were recorded for both complexes in acetonitrile solutions (10^{-5} M) with an F-7000 FL spectrophotometer. The photoluminescence quantum yields (PLQYs) of the complexes in solution were measured with $[Ru(bpy)_3]Cl_2$ in water (Φ_r = 0.04) as the reference substance. Electrochemical measurements were performed in acetonitrile solution (10^{-3} M) using a potentiostat/galvanostat (Iviumstat) voltammetric analyzer at a scan rate of 100 m V s^{-1}. The electrolytic cell consisted of a glassy carbon electrode, platinum wire, and Ag/AgCl as the working, counter, and reference electrodes, respectively. Ferrocene was added as an internal standard and tetrabutylammonium hexafluorophosphate ($TBAPF_6$) in acetonitrile solution (0.1 M) served as the supporting electrolyte. The energy values of the highest occupied molecular orbital (E_{HOMO}), the lowest unoccupied molecular orbital (E_{LUMO}), and the electrochemical bandgaps (E_g) of the complexes were calculated using the empirical relation [28,29]: $E_{HOMO} = [-e(E_{ox(vs.\ Ag/AgCl)} - E_{1/2\ (Fc/Fc^{+}\ vs.\ Ag/AgCl)})] - 4.8$ eV, $E_{LUMO} = [-e(E_{red} - E_{1/2})] - 4.8$ eV and $E_g = E_{HOMO} - E_{LUMO}$. Here, E_{ox} and E_{red} are the oxidation and reduction potentials respectively, whereas $E_{1/2\ (Fc/Fc^{+}\ vs.\ Ag/AgCl)}$ is the redox potential of ferrocene, which was found to be 0.43 V. The surface morphology of the films and their root-mean-square (rms) roughness were measured by atomic force microscopy (AFM; Hitachi High Tech Science NanoNavi/L-trace II). The films were prepared on an ITO/PEDOT:PSS surface by spin-coating the complexes from acetonitrile solution. The film formation process is explained in detail in Section 2.6. “LEC Device Fabrication and Characterization”.

2.2. Synthesis of 2-(quinolin-2-yl)-1-(p-tolyl)-1H-phemnanthro[9,10-d] imidazole (Qtpi)

The ancillary ligand Qtpi was synthesized according to the literature procedure [30–32]. Quinoline-2-carboxaldehyde (1.10 g, 7 mmol) and *p*-toluidine (0.75 g, 7 mmol) were dissolved in 15 mL of glacial acetic acid and stirred for 20 min at room temperature. 9,10-Phenanthrenequinone (1.46 g, 7 mmol) and ammonium acetate (539 g, 70 mmol) were added to the reaction mixture and refluxed under argon atmosphere for 24 h. After cooling to room temperature, the reaction mixture was extracted with water and dichloromethane. The organic layer was then dried over anhydrous Na_2SO_4 and concentrated under vacuum. The crude product was loaded onto a silica gel column and eluted with hexane/ethylacetate (9:1) to give the product as a yellow solid. ^1H NMR (500 MHz, CD_2Cl_2) δ (ppm): 892 (d, *J* = 7.91 Hz, 1H), 8.77 (d, *J* = 8.17 Hz, 1H), 8.71 (d, *J* = 8.15 Hz, 1H), 8.44 (d, *J* = 8.59 Hz, 1H), 8.18 (d, *J* = 8.61 Hz, 1H), 7.79–7.73 (m, 2H), 7.70–7.64 (m, 1H), 7.62–7.59 (m, 1H), 7.56–7.52 (m, 2H), 7.50–7.46 (m, 3H), 7.40 (d, *J* = 7.89 Hz, 2H), 7.35–7.27 (m, 2H), 2.59 (m, 3H).

Anal. Calcd. (%) for $C_{31}H_{21}N_3$: C, 85.49; H, 4.86; N, 9.65. Found: C, 85.56; H, 4.79; N, 9.56. ESI^+ TOF MS: *m/z* 436.2 ({M + H}$^+$, 100%).

2.3. Synthesis of $[Ir(ppy)_2(Qtpi)]PF_6$ (complex 1)

The dichloro-bridged dimeric iridium complex, $[Ir(ppy)_2Cl]_2$ (108 mg, 0.1 mmol) and Qtpi (100 mg, 0.23 mmol) were heated to reflux in dichloromethane/methanol (15/15 mL) at 60 °C under argon atmosphere for 18 h. The obtained orange solution was cooled to room temperature. The chloride complexes were then treated with solid NH_4PF_6 (65 mg, 0.4 mmol) for 1 h at room temperature to replace Cl^- with PF_6^-. The orange solution was evaporated to dryness to afford an orange solid, which was dissolved in the minimum amount of dichloromethane to remove the insoluble inorganic impurities. Crystals of the complexes were grown by the slow diffusion of diethyl ether into a concentrated solution of the compound in dichloromethane. Yield: 178 mg, 0.15 mmol, 77%. ^{1}H NMR (500 MHz, CD_2Cl_2) δ (ppm): 8.67 (d, J = 8.29 Hz, 1H), 8.50 (d, J = 8.33 Hz, 1H), 8.32 (d, J = 6.61 Hz, 1H), 8.23 (d, J = 8.76 Hz, 1H), 8.07 (dd, J = 8.10, 1.10 Hz, 1H), 8.01–7.91 (m, 4H), 7.86–7.79 (m, 2H), 7.75–7.69 (m, 6H), 7.67–7.60 (m, 2H), 7.53–7.48 (m, 1H), 7.47–7.43 (m, 1H), 7.40–7.36 (m, 1H), 7.35–7.30 (m, 1H), 7.28–7.17 (m, 3H), 7.12–7.01 (m, 4H), 6.99–6.89 (m, 2H), 6.87–6.79 (m, 2H), 2.69 (s, 3H). ^{13}C NMR (126 MHz, CD_2Cl_2) δ (ppm): 167.8, 154.2, 150.9, 148.7, 144.6, 143.9, 141.2, 137.9, 137.6, 137.0, 134.2, 132.7, 131.4, 130.6, 129.2, 128.9, 128.4, 127.8, 127.5, 127.1, 126.8, 126.4, 125.8, 124.3, 123.6, 122.4, 122.1, 120.7, 119.5, 21.8. Anal. Calcd (%) for $C_{53}H_{37}N_5PF_6Ir$: C, 58.88; H, 3.50; N, 6.48. Found: C, 58.83; H, 3.59; N, 6.41. ESI^+ TOF MS: *m/z* 936.3 ({M –PF_6^+, 100%).

2.4. Synthesis of $[Ir(piq)_2(Qtpi)]PF_6$ (complex 2)

The synthesis of Complex 2 was analogous to that of Complex 1, but $[Ir(ppy)_2Cl]_2$ was replaced by $[Ir(piq)_2Cl]_2$. Yield: 200 mg, 0.17 mmol, 85%. ^{1}H NMR (500 MHz, CD_2Cl_2) δ (ppm): 9.07 (d, J = 8.41 Hz, 1H), 8.61 (d, J = 8.22 Hz, 1H), 8.55 (d, J = 6.42 Hz, 1H), 8.49 (dd, J = 8.11, 3.12 Hz, 2H), 8.20 (d, J = 8.79 Hz, 1H), 8.03–7.93 (m, 4H), 7.90–7.74 9m, 7H), 7.72 (d, J = 8.94 Hz, 1H), 7.67 (d, J = 7.63 Hz, 2H), 7.62–7.38 (m, 8H), 7.33 (d, J = 6.39 Hz, 1H), 7.30–7.13 (m, 4H), 7.10 (d, J = 8.80 Hz, 1H), 7.02 (dd, J = 7.98, 2.29 Hz, 1H), 6.95–6.87 (m, 2H), 6.85–6.80 (m, 1H), 2.65 (s, 3H). ^{13}C NMR (126 MHz, CD_2Cl_2) δ (ppm): 169.5, 169.2, 153.8, 151.4, 150.3, 148.9, 147.7, 146.2, 146.0, 143.7, 143.2, 141.5, 140.6, 137.7, 137.0, 136.7, 134.1, 133.3, 133.1, 132.9, 132.2, 131.9, 131.1, 130.4, 129.5, 129.2, 128.6, 128.4, 128.1, 127.9, 127.0, 126.4, 125.9, 124.6, 123.5, 122.9, 121.7, 121.3, 120.9, 117.5, 21.9. Anal. Calcd. (%) for $C_{61}H_{41}N_5PF_6Ir$: C, 62.03; H, 3.50; N, 5.93. Found: C, 61.94; H, 3.58; N, 5.86. ESI^+ TOF MS: *m/z* 1036.3 ({M –PF_6}$^+$, 100%).

2.5. Quantum chemical calculations

Density functional theory (DFT) and time-dependent DFT (TDDFT) methods were used to calculate the ground and excited state properties of the two Ir complexes using the Gaussian 09 program [33]. First, the geometries of the two complexes were optimized in the gas phase and harmonic vibrational frequency analysis was then carried out to ensure no imaginary frequencies. The hybrid exchange-correlation B3LYP [34–36] functional was employed in combination with the 6-31G(d) basis set for all the lighter atoms (H, C, and N). A "double-ξ" quality basis set consisting of Hay and Wadt's effective core potentials (LanL2DZ ECP) [37–39] was used for the Ir atom. The optimized geometries were then subjected to TDDFT simulations to obtain the UV–-visible absorption spectra. To mimic the experimental conditions, the implicit polarizable continuum model (PCM) was used to account for the solvent (acetonitrile) effects, as implemented in Gaussian 09.

2.6. LEC device fabrication and characterization

All materials were used as received. The buffer layer material, poly (3,4-ethylenedioxythiophene):polystyrenesulfonate (PEDOT:PSS) was purchased from Heraeus Clevios (P VP Al 4083). Prior to deposition, PEDOT:PSS was filtered using a 0.2-μm hydrophilic PTFE–filter. The hole conducting material, PEDOT:PSS was used to avoid the formation of pinholes and to improve the yield and reproducibility of the LEC devices. The indium tin oxide (ITO) glass substrates, patterned using conventional photolithography, were obtained from Samsung Corning, South Korea.

The LECs were fabricated as follows. The ITO glass plates were washed in a mixture of solvents containing acetone, ethanol, and isopropyl alcohol (1:1 v/v) for 30 min using an ultrasonic bath. The substrates were then UV–ozone treated for 30 min. Prior to deposition of the active layer, a 50-nm-thick film of PEDOT:PSS was spin-coated onto the pre-cleaned ITO substrates at 2000 rpm for 20 s and dried for 20 min at 120 °C in a vacuum oven. The emitting layer was then spin-coated from acetonitrile solution (1 mL) containing 20 mg of complexes to produce a smooth film with a thickness of approximate 70 nm. The film was then baked at 80 °C for 1 h in a vacuum oven. The substrates were then transferred into a metal-evaporating chamber and a 100-nm-thick film of aluminum was deposited as the cathode using a shadow mask under high vacuum. The configuration of the ultimate device was as follows: ITO/PEDOT:PSS/iTMCs/Al. The electroluminescence properties of the devices were analyzed using Keithley characterization systems under ambient conditions. The luminescence and current density versus voltage characteristics of the LEC devices were evaluated using a Keithley 2400 source meter and calibrated with a silicon photodiode. An Avantes luminance spectrometer was used to acquire the EL spectrum and Commission Internationale de L'Eclairage (CIE) coordinates.

3. Results and discussion

3.1. Synthesis and characterization

The quinolin-imidazole-based ancillary ligand (Qtpi) was synthesized in a one-step reaction according to the method presented by Debus and Radziszewsk [32]. Qtpi was used due to the intriguing photophysical properties of the imidazole derivatives fused with the phenanthroline ring and quinolone group. The cationic iridium complexes of the type $[Ir(C^N)_2(N^N)]^+PF_6^-$ were synthesized by cleavage of the corresponding cyclometalated Ir^{III} μ-dichloro-bridged dimer, $[Ir(C^N)_2(\mu\text{-}Cl)]_2$ based on Hppy or Hpiq with the Qtpi ancillary ligand in dichloromethane/methanol [40]. The chloride complexes thus obtained underwent ion metathesis reaction with excess of NH_4PF_6 to form cationic iridium complexes in high yields. All complexes were fully characterized by elemental analysis, ^{1}H, ^{13}C NMR spectroscopy, and mass spectrometry. The synthetic routes, along with the structures of the ancillary ligand and cationic iridium complexes, are displayed in Scheme 1.

3.2. Photophysical properties

The optical properties of the cationic iridium complexes were studied by means of absorption and emission spectroscopy. The UV–visible absorption spectra of the complexes in acetonitrile solution (10^{-5} M) are shown in Fig. 1. All the complexes showed intense absorption bands ($\varepsilon > 3.7 \times 10^4$ M^{-1} cm^{-1}) below 300 nm, attributed to spin-allowed ligand-centered (LC) $^1\pi$—π^* transitions of both the cyclometalated and ancillary ligands. Spin-allowed metal-to-ligand charge transfer (^{1}MLCT) and ligand-to-ligand charge transfer (^{1}LLCT) transitions with moderate intensity were observed in the range of 300–400 nm. The very low intensity tails ($\varepsilon < 0.65 \times 10^4$ M^{-1} cm^{-1}) above 400 nm extending toward the visible region arise from the spin-forbidden ^{3}LLCT, ^{3}LC, and

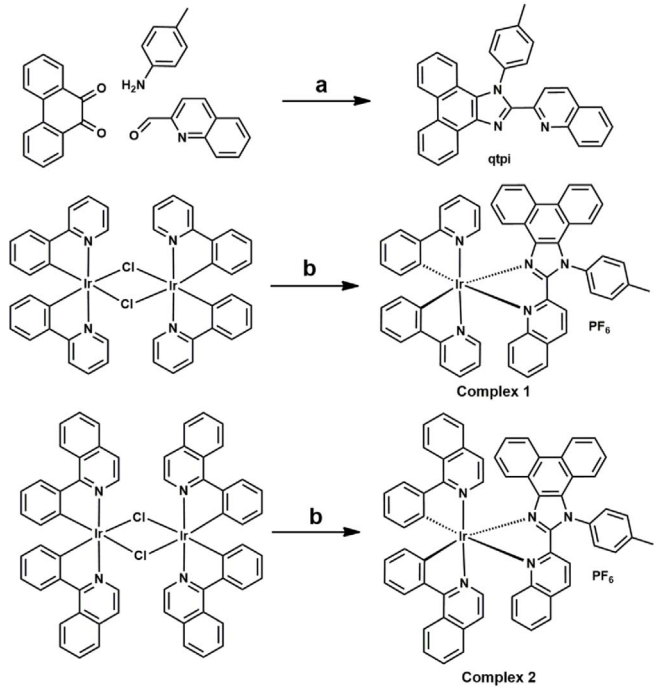

Scheme 1. Synthesis of Qtpi ancillary ligand and cationic iridium complexes (Complex 1 and Complex 2). *Reaction conditions*: (a) ammonium acetate, glacial acetic acid, reflux, 24 h, under Ar; (b) **qtpi**, CH_2Cl_2/CH_3OH, 60 °C, 18 h, under Ar, NH_4PF_6.

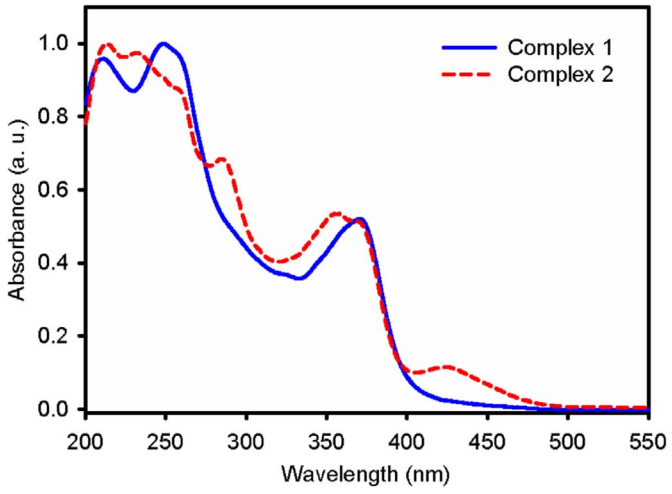

Fig. 1. Room temperature UV–visible absorption spectra of Complex 1 and Complex 2 in dilute acetonitrile solution (10^{-5} M).

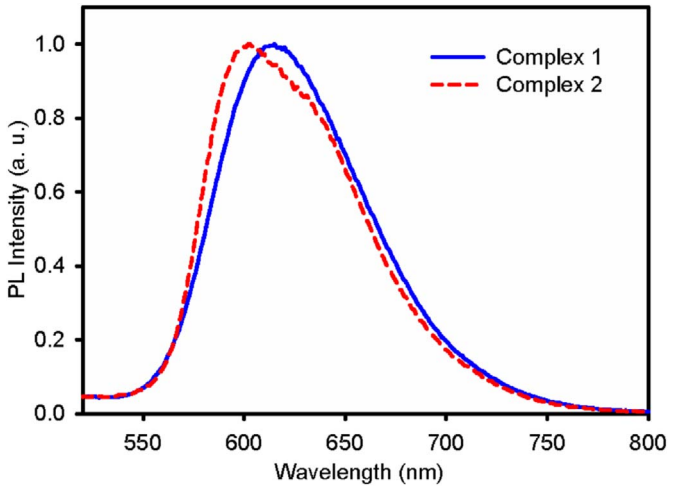

Fig. 2. Room-temperature normalized photoluminescence (PL) emission spectra of Complex 1 and Complex 2 in acetonitrile solution (10^{-5} M) upon excitation at 490 nm.

^{3}MLCT transitions of the complexes [41]. The spin-forbidden transitions (^{3}MLCT, ^{3}LLCT, and ^{3}LC) gained substantial intensity due to the strong spin–orbit coupling caused by the heavy iridium center, which enables the mixing of low lying triplet states with higher-lying ^{1}MLCT states [40,42]. The absorption wavelengths and corresponding molar extinction coefficients of Complex 1 and Complex 2 are summarized in Table 1. The absorption spectrum of Complex 2 showed more intense absorption bands; these were significantly red-shifted compared to that of Complex 1. The observed bathochromic shift can be ascribed to the presence of extended π-conjugation on the phenylpyridine ligand of Complex 2.

The photoluminescence (PL) emission spectra of the complexes in acetonitrile solution are presented in Fig. 2. The emission spectrum of Complex 1 displayed structureless transition bands, whereas that of Complex 2 displayed vibronically structured emission at room temperature. The featureless emission spectrum of Complex 1 is due to the ^{3}MLCT electronic excitations, whereas the vibronically structured emission indicates that the emissive excited states of Complex 2 have predominantly LC $^3\pi$–π^* character rather than ^{3}MLCT or ^{3}LLCT character [40,42,43]. In acetonitrile solution, Complex 1 showed orange emission with a maximum at 614 nm. However, Complex 2 exhibited orange-red emission with an emission maximum at 603 nm and a shoulder at 630 nm. The emission spectrum of Complex 2 was slightly shifted toward longer wavelengths compared to that of Complex 1, which is due to the presence of extended conjugation on the cyclometalated ligands, which raises the HOMO energy level of Complex 2. The emission quantum yields (Φ) of the complexes were measured in degassed acetonitrile solution. The quantum yields of Complex 1 and Complex 2 were 0.16 and 0.09, respectively. The photoluminescence of

Table 1
Photophysical, thermal, and electrochemical characteristics of Complex 1 and Complex 2.

Complex	λ_{abs}[a] [nm] (ε [× 10^4 M^{-1} cm^{-1}])	Emission at room temperature				T_d (°C)	Electrochemical data[e]		
		Solution[b] λ [nm]	Film[c] λ [nm]	Φem[d]			E_{ox} [V]	E_{red} [V]	E_{gap} [eV]
				CH_3CN	Film				
1	213 (5.5), 250 (5.8), 372 (2.9), 442 (0.11)	614	600	0.16	0.12	200	1.05	−1.96	3.01
2	215 (5.4), 233 (5.3), 258 (4.7), 286 (3.7), 356 (2.9), 371 (2.7), 429 (0.65), 492 (0.07)	603, 630 sh	614 sh, 642	0.09	0.06	203	1.02	−1.69	2.71

[a] Absorption wavelength and molar extension coefficients.
[b] Maximum emission wavelength, measured in acetonitrile solution at 10^{-5} M; sh denotes the shoulder wavelength.
[c] Neat films were made on quartz substrate.
[d] PL quantum yield of complexes in acetonitrile solution, measured with $[Ru(bpy)_3]Cl_2$ in water (Φ_r = 0.04). T_d represents the decomposition temperature.
[e] Electrochemical data versus Fc^+/Fc (Fc indicates ferrocene) measured in 10^{-3} M acetonitrile solution.

the complexes display single exponential decay in acetonitrile solution with excited state lifetimes (τ) of 0.59 μs and 0.51 μs for Complex 1 and Complex 2, respectively (Fig. S1). The excited state lifetimes of both complexes are comparable due to their structure similarity. On the basis of τ and Φ, the radiative (K_r) and non-radiative decay rates have been calculated for both complexes. The K_r calculated for Complex 1 and Complex 2 in degassed acetonitrile solutions are $2.71 \times 10^5$and 1.76×10^5 s^{-1}, respectively, whereas their K_{nr} calculated are 1.42×10^6 and 1.78×10^6 s^{-1}, respectively. The K_r value of Complex 2 is smaller than Complex 1 indicates less ^{3}MLCT character for the emissive excited state of Complex 2.

The PL emission spectra of complexes in neat films have also been investigated and displayed in Fig. S2 in the supporting information. The detailed emission characteristics are summarized in Table 1. The PL spectra of complexes in neat film resemble to those in solutions. However, the film PL spectrum of Complex 1 is blue-shifted to some extent (600 nm), whereas that of Complex 2 is red-shifted with an emission maximum at 642 nm and a shoulder peak at 614 nm. The thin film emission spectrum of Complex **2** shows much wider and structured emission band, indicate the dominant LC $^3\pi$–π^* character. Moreover, the long tail extending to 850 due to the strong intermolecular interactions in neat films of Complex 2 than in the solution. The PLQYs of neat films of Complexes 1 and 2 were also measured and shown in Table 1. The PLQY values of complexes in neat films are 0.12 and 0.06 for Complex 1 and 2, respectively. The decreased PLQY values of thin films of Complex 1 and 2, indicating severe excited-state quenching in neat films.

3.3. Thermal and electrochemical properties

The thermal properties of the complexes were investigated by thermogravimetric analysis (TGA) and the TGA curves are shown in Fig. 3. The complexes underwent two-step decomposition above 200 °C and no weight loss was observed for either complex upon heating to 200 °C under nitrogen. Both complexes showed excellent thermal stability, which is required for their use as the active layer in LECs. The decomposition temperatures (T_d) of Complex 1 and 2 are summarized in Table 1.

The electrochemical properties of the complexes were studied by cyclic voltammetry (CV) measurements in acetonitrile solution using a 0.1 M solution of tetrabutylammonium hexafluorophosphate ($TBAPF_6$). The cyclic voltammograms of Complexes 1 and 2 are displayed in Fig. 4 and the redox potentials are summarized in Table 1. As shown in Fig. 4, Complex 1 and 2 respectively showed irreversible oxidation waves with oxidation potentials at 1.05 and 1.02 V. The oxidation waves are

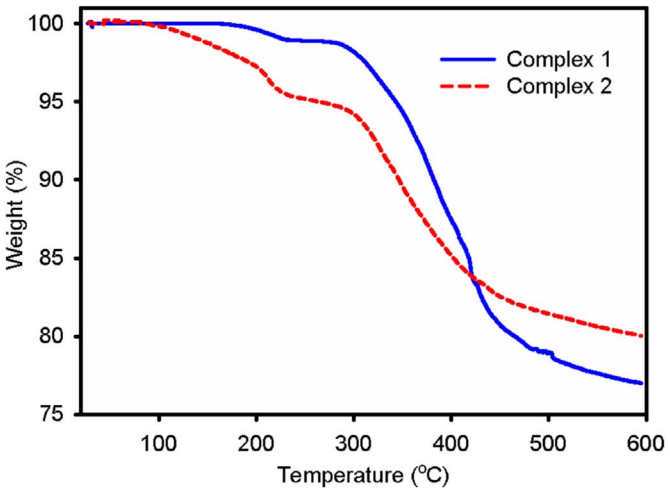

Fig. 3. TGA curves of Complex 1 and Complex 2, acquired at a heating rate of 20 °C min^{-1} under nitrogen.

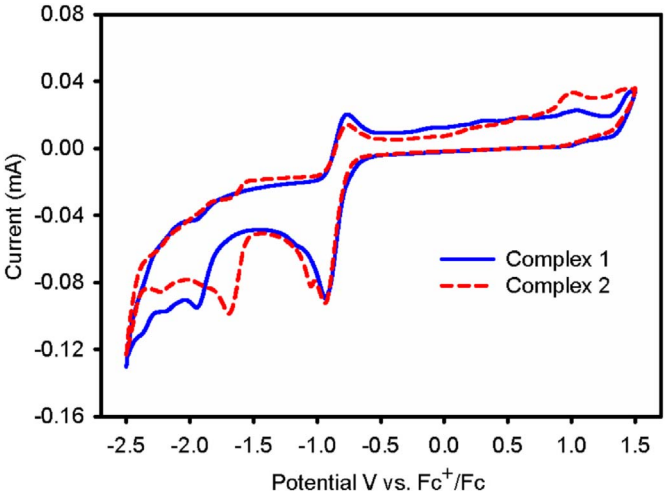

Fig. 4. Cyclic voltammograms of Complex 1 and Complex 2 recorded in 0.1 M $TBAPF_6$ in acetonitrile solution versus Fc^+/Fc (ferrocenium/ferrocene) at a scan rate of 100 mV s^{-1}.

attributed to the oxidation of Ir(III) to Ir(IV) with slight involvement of the cyclometalated ligands on which the HOMO resides. Similarly, Complex 1 and Complex 2 respectively exhibited irreversible reduction peaks with reduction potentials of −1.96 and 1.69 V. The reduction waves are attributed to the reduction of the ancillary ligand, with involvement of the cyclometalating ligands. Notably, the reduction potential of Complex 2 was anodically shifted by 270 mV compared to that of Complex 1. This is due to the electron-rich nature of the Piq cyclometalating ligands on Complex 2, which makes reduction much easier than in the case of Complex 1. The HOMO and LUMO energy levels and the corresponding energy gaps of the complexes were calculated from the corresponding oxidation and reduction potentials using the empirical relations. The HOMO energies calculated for Complexes 1 and 2 were −5.42, and −5.39 eV, respectively, and the LUMO energies were −2.41 and −2.68 eV, respectively. Notably, the use of Piq and Qtpi ligands in Complex 2 resulted in destabilization of the HOMO as well as stabilization of the LUMO, thereby narrowing the energy-gap for Complex 2 (2.71 eV) relative to that of Complex 1 (3.01 eV). Since the LUMO of Complex 2 is more stabilized compared to that of Complex 1, thereby result larger energy difference between the LUMO and antibonding metal center (*MC) state for Complex 2 than Complex 1. Hence the population of *MC state is hardly occur for Complex 2, which is naturally unstable and their population results complex degradation during device operation [19]. Therefore Complex 2 is expected to exhibit higher stability when utilized in LECs.

3.4. Quantum chemical calculations

Because the molecular geometries of the complexes significantly impact their electrochemical and photophysical properties, DFT calculations were performed to gain deeper insight into the structural properties. The optimized ground-state geometries of the two Ir complexes are presented in Fig. 5. The two phenylpyridine ligands and the Qtpi ancillary ligand around the Ir metal center confer a pseudo-octahedral geometry to the complexes. The Ir-C cyclometalated bond is the shortest bond around the metal center, with a bond length of 2.02 Å. On the other hand, the Ir-N bond distance (~2.08 Å) for the phenylpyridine ligand is shorter than that of the Qtpi ancillary ligand (~2.35 Å). The bond angle of the phenyl pyridine ligand with Ir is ~80° and that of the ancillary ligand with Ir is ~73°. The planarity of the phenyl pyridine ligands is disrupted in Complex 1 relative to Complex 2 because of the added phenyl ring. The methylbenzene attached to the imidazole of the ancillary ligand lies perpendicular to the rest of the moiety.

To examine the charge transfer phenomenon, population analysis

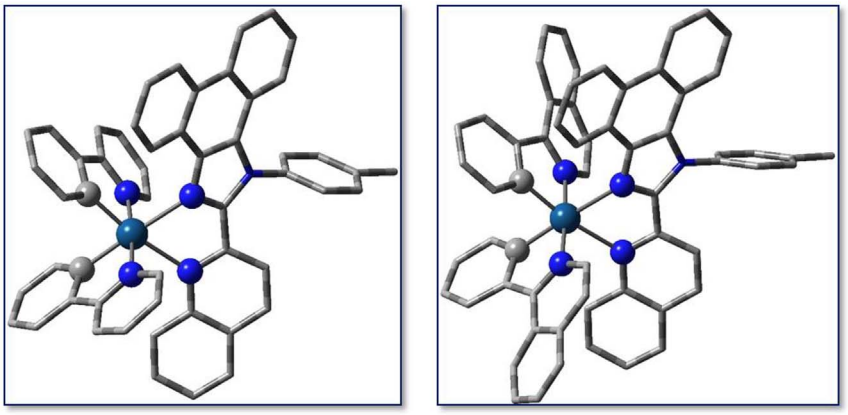

Fig. 5. Ground state geometries of Complexes 1 (left) and 2 (right) obtained at B3LYP/6-31G(d)/LanL2DZ level of theory. Hydrogen atoms are omitted for clarity.

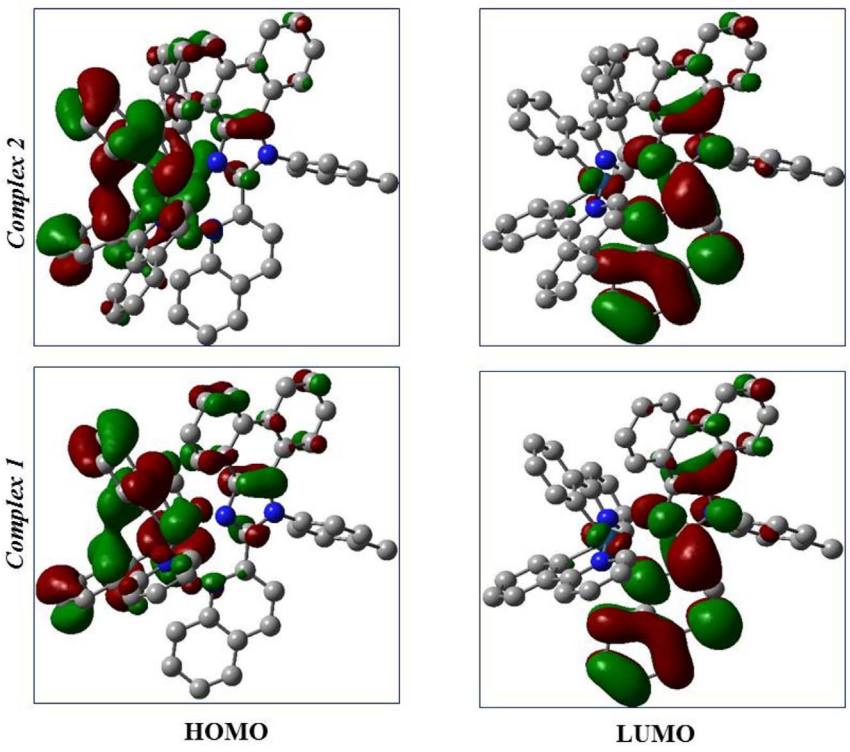

Fig. 6. Electron density distribution pattern of the frontier molecular orbitals for Complex 1 (bottom) and 2 (top), obtained at B3LYP/6-31G(d)/LanL2DZ level of theory.

Table 2
Simulated electrochemical data and TDDFT transition energies ($E_{0\text{-}0}$) of the two complexes.

Complex	**1** (eV)	**2** (eV)
HOMO	−5.69	−5.66
LUMO	−2.54	−2.55
HOMO-LUMO gap	3.15	3.11
$E_{0\text{-}0}$	2.51	2.47

was carried out for the frontier molecular orbitals. The electron density distribution pattern in the HOMO and LUMO of the two Ir complexes is presented in Fig. 6. In the HOMOs of the complexes, the electron density is mainly localized over the two phenyl pyridine ligands and the Ir metal center. In the LUMOs of the complexes, the electron density is shifted to the ancillary ligand. The calculated electrochemical data and the TDDFT transition energy, i.e., optical bandgap, are listed in Table 2. The calculated eigenvalues of the frontier molecular orbitals of the two complexes are in very good agreement with those obtained from the experimental cyclic voltammetry data. The HOMO energy for Complex 2 was slightly higher than that of Complex 1, whereas the LUMO energy remained almost unchanged. The trend observed for the HOMO-LUMO gap matches well with the experimental bandgap. Interestingly, the decrease in the electrochemical bandgap and optical bandgap was identical for Complex 1 and Complex 2 (0.04 eV). Because of the decreased bandgap, bathochromic shifts in the optical absorption and emission of the complexes are expected.

TDDFT simulations were carried out to evaluate the vertical excitation energies and photophysical behavior of the two Ir complexes. The calculated UV–visible absorption spectra of the complexes acquired in acetonitrile solution are portrayed in Fig. 7. The optical data of the first five singlet excitations are summarized in Table 3. The experimentally observed main absorption bands were reproduced in the TDDFT simulations. As expected, a considerable bathochromic shift was observed for Complex 2 relative to Complex 1. The observed bathochromic shift can be attributed to the lowered bandgap due to the extended π-conjugation on the phenyl pyridine ligand in Complex 2. The most intense singlet transition in the low energy region (*ca.* 500 nm) for each complex arises mainly from HOMO → LUMO excitation. The simulated absorption data are in good agreement with the

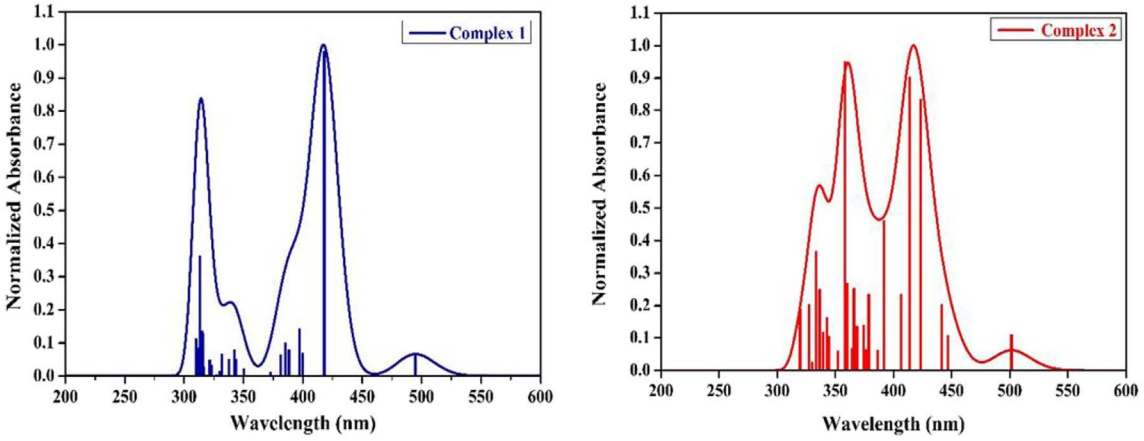

Fig. 7. Theoretically obtained UV–visible absorption spectra of Complex 1 and 2, calculated at B3LYP/6-31G(d)/LanL2DZ level of theory.

experimental UV–visible absorption spectra.

3.5. Electroluminescence properties of LECs

LECs were fabricated to investigate the electroluminescence properties of the two synthesized iridium complexes. The configuration of the fabricated devices was as follows: ITO/PEDOT:PSS//iTMC/Al. The PEDOT:PSS layer was introduced in-between the ITO and iTMC layers, not only to smoothen the ITO surface, but also to promote hole injection [43].

Smooth and homogeneous surfaces of thin films of iridium complexes are essential for the fabrication of efficient LEC devices. In order to study the film-forming ability of the iridium complexes, AFM measurements were conducted. The films were made by spin-coating the complexes onto the surface of an ITO glass substrate with a PEDOT:PSS layer. The AFM images of both complexes (Fig. 8) demonstrate a smooth surface morphology with respective root mean square (rms) roughness values of 0.44 and 2.37 nm for Complex 1 and Complex 2. The rms value of Complex 1 was lower than that of Complex 2, leading to efficient charge combination, and consequently, better device efficiency. However, holes and buds were apparent on the surface of the films of both complexes, which may deteriorate the device performance [44]. It might be due to the aggregation of particle during spin coating process followed by the fast drying of solvent.

The electroluminescence (EL) spectra of LECs based on Complex 1 and 2 are shown in Fig. 9. The LECs based on both complexes emitted in the red region of the visible spectrum. As shown in Fig. 9, the EL spectra of the complexes presented a broad emission and a long tail extending to the near-infrared region. Apart from the broad EL spectrum, the spectrum of the LECs utilizing Complex 1 resembled the PL emission spectrum in solution, with an emission peak at 618 nm and CIE coordinates of (0.59, 0.36). The broad EL emission bands of Complex 1 are attributed to the strong intermolecular interactions in the thin solid films. However, the EL spectrum of Complex 2 showed featureless emission that differed from the PL spectrum, with an emission maximum centered at 692 nm and CIE coordinates of (0.56, 0.28). The featureless EL spectrum of Complex 2 indicates that the emission arises from the LC state rather than from CT. Moreover, the EL spectrum of Complex 2 was significantly red-shifted (by 72 nm) relative to the PL spectrum, attributed to electrical excitation, which might cause polarization of the molecular orbitals, excimer formation, or chemical changes in the complexes under high electric fields [45,46]. The EL spectrum of Complex 2 was largely shifted to the longer wavelength region due to extended conjugation on the cyclometalated ligands, which lowers the energy-gap to a larger extent than in the case of Complex 1. These results demonstrate that the phenanthroimidazole derivative is a promising ligand for tuning the emission color of Ir complexes to the red region of the visible spectrum.

The luminance-voltage and current density-voltage curves of the LECs based on Complex 1 and 2 are presented in Fig. 10, and the key performance parameters are summarized in Table 4. The device was scanned with a sweep rate of 0.5 V/s. Upon applying a bias to the device, the luminance and current density increased slowly with the voltage, which is a typical characteristic of LECs, reflecting the lethargic movement associated with the slow migration of PF_6^- ions and cationic counterparts towards the anode and cathode, respectively. Complexes of Ir(IV)/Ir(III) (p type) were formed in a region near the anode, where the iridium complexes are oxidized, whereas Ir(III)/Ir(II) complexes (n-type) were created in a region near the cathode. As a result, charge injection from the electrode surfaces occurred, and the more balanced recombination resulted in improved luminance and current efficiency for the devices as a function of the voltage.

Notably, the luminance and current density of the devices increased slowly up to 6 V and then increased abruptly, reaching a maximum luminance of 808 and 525 cd m^{-2} and current density of 110 and 262 mA cm^{-2} for Complex 1 and 2 respectively. The LECs based on

Table 3
Simulated TDDFT data for the first five excited states of the two complexes, obtained at TD-B3LYP/6-31G(d)/LanL2DZ level of theory.

Complex	λ_{cal} (nm)	Excitation State	*f*	CI Coefficient	Dominant Contribution (%)
1	495	$S_0 \rightarrow S_1$	0.0258	0.6914	HOMO → LUMO (96)
	418	$S_0 \rightarrow S_2$	0.3741	0.6780	HOMO-1 → LUMO (92)
	400	$S_0 \rightarrow S_3$	0.0263	0.4994	HOMO → LUMO+1 (50)
	397	$S_0 \rightarrow S_4$	0.0547	0.4638	HOMO → LUMO+1 (74)
	388	$S_0 \rightarrow S_5$	0.0306	0.6625	HOMO-2 → LUMO (88)
2	501	$S_0 \rightarrow S_1$	0.0210	0.6894	HOMO → LUMO (95)
	447	$S_0 \rightarrow S_2$	0.0204	0.6415	HOMO → LUMO+1 (82)
	442	$S_0 \rightarrow S_3$	0.0389	0.6317	HOMO → LUMO+2 (80)
	423	$S_0 \rightarrow S_4$	0.1592	0.6127	HOMO-1 → LUMO (75)
	414	$S_0 \rightarrow S_5$	0.1725	0.6026	HOMO-2 → LUMO (73)

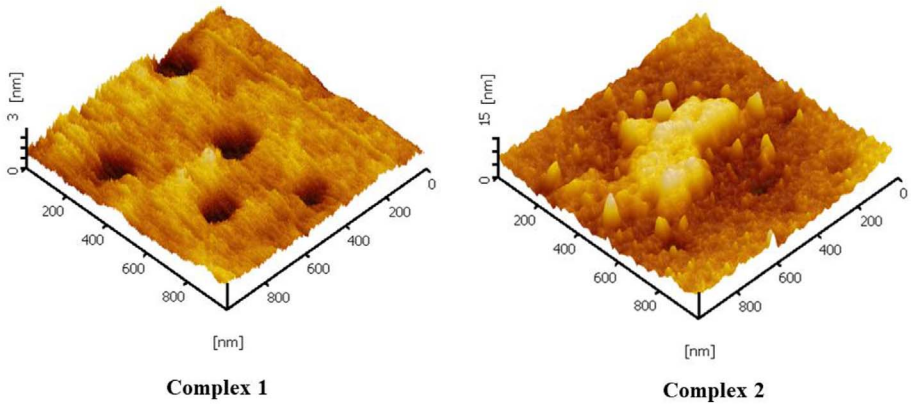

Fig. 8. AFM images of thin films of (a) Complex 1 and (b) Complex 2 deposited on top of PEDOT:PSS/ITO layer.

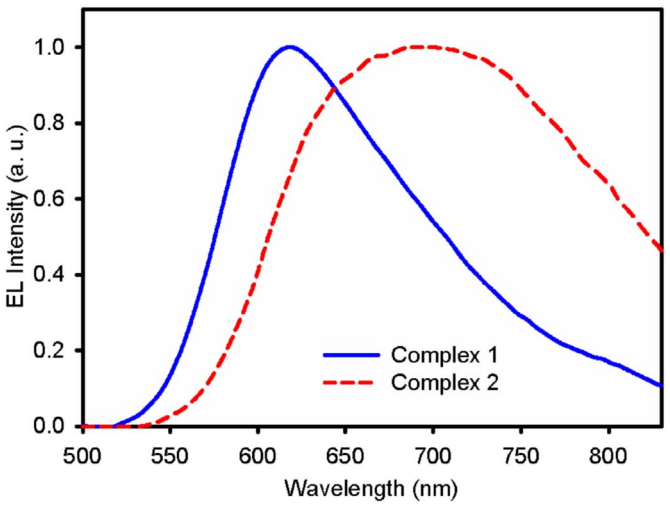

Fig. 9. Electroluminescence (EL) spectra of LECs based on Complexes 1 and 2.

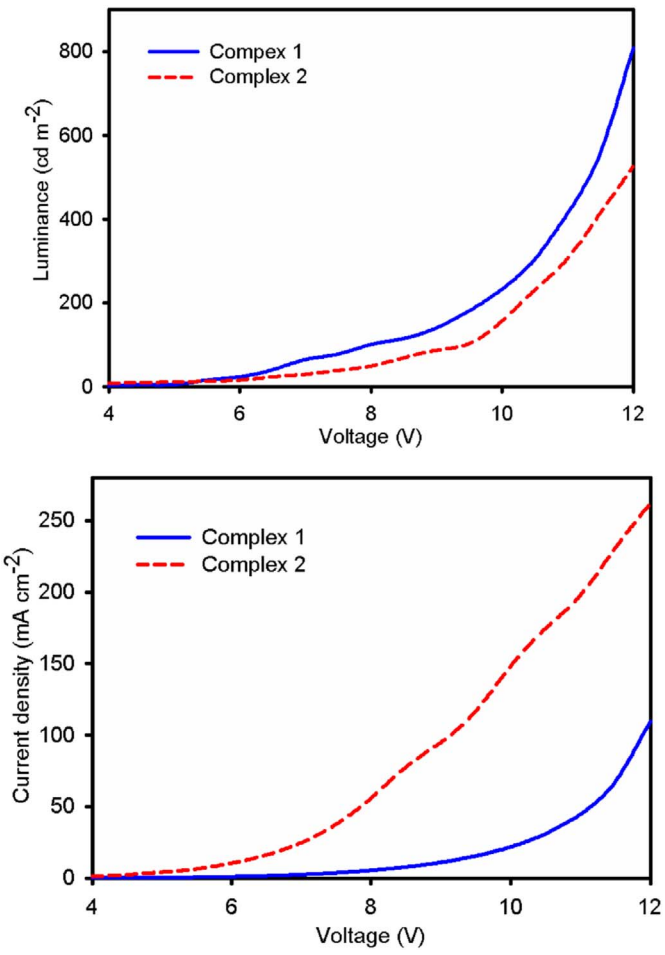

Fig. 10. Voltage-dependent luminance and current density curves of LECs based on Complex 1 and 2.

Complex 1 exhibited a higher current efficiency of 0.73 cd A^{-1} than that (0.20 cd A^{-1}) obtained with Complex 2. The efficiency of the LECs incorporating Complex 2 was more strongly affected by the increasing current density than that of Complex 1. The inferior device performance achieved with Complex 2 is due to the presence bulky phenyl groups on both the cyclometalated and ancillary ligands, which may hinder charge transport between the complexes or reduce the ionic conductivity. However, the presence of bulky substituents or π–π stacking interaction on the ancillary ligand plays a pivotal role in maintaining the device stability by diminishing the intermolecular interaction between the iridium complexes, thereby hindering the water-induced substitution reaction and non-radiative pathways. The device performances of some reported red-emitting iTMCs-LECs are summarized in Table 4. As shown in Table 4, LECs based on red-emitting iridium complexes exhibit higher brightness and current efficiency than that of ruthenium complexes. Moreover, the reported iridium complexes show superior device stability than ruthenium complexes due to the large energy difference between ^{3}MLCT and metal centered (^{3}MC) states, thereby impeding the population of ^{3}MC state and prevents the complex degradation during device operation [19,20].

4. Conclusions

Two novel phenanthroimidazole-based cationic iridium complexes, $[Ir(ppy)_2(Qtpi)]PF_6$ (Complex 1) and $[Ir(piq)_2(Qtpi)]PF_6$ (Complex 2), were synthesized and characterized. The extended conjugation in Complex 2 resulted in significant destabilization of the HOMO orbitals and stabilization of the LUMO orbitals, resulting in a narrower energy-gap and consequently red-shifted emission compared to Complex 1. LECs were fabricated, demonstrating red emission from both complexes, centered at 618 and 692 nm for Complexes 1 and 2, respectively. The red-emitting LEC based on these complexes showed maximum luminance and current efficiency values of 808 cd m^{-2} and 0.73 cd A^{-1} for Complex 1 and 525 cd m^{-2} and 0.20 cd A^{-1} for Complex 2, respectively. Moreover, the complexes exhibited high device stability with increasing voltage, which may be due to the presence of bulky substituents or π–π stacking interactions on the ancillary ligand, resulting in a less populated ^{3}MC state, thereby hindering the water-induced substitution reaction and non-radiative pathways. These results suggest that cationic iridium complexes with ancillary phenanthroimidazole ligands are promising electroluminescent materials for

Table 4
Comparison of electroluminescent properties of red-emitting iTMCs-LECs based on ruthenium and iridium complexes.

Complex	Lum_{max} [cd m^{-2}]	Current $density_{max}$ [mA cm^{-2}]	Current efficiency (cd A^{-1})	EL_{max} (nm)	CIE coordinates	Ref.
1 (Ru)	86	n/a	0.012	637	n/a	[47]
2 (Ru)	133	n/a	0.074	657	n/a	[47]
3 (Ru)	38	n/a	0.010	678	n/a	[47]
4 (Ru)	47	n/a	0.015	655	n/a	[47]
$[Ru(phen)_3](BF_4)_2$	120	n/a	0.084	670	(0.63, 0.37)	[48]
$[Ru(phen)_2$ Lhydro$](BF_4)_2$	350	n/a	0.417	670	(0.64, 0.36)	[48]
1 (Ir)	59	n/a	n/a	661	(0.65, 0.34)	[21]
$[Ir(bzq)_2(biq)]PF_6$	33.65	n/a	0.33	662	n/a	[19]
1 (Ir)	77	n/a	0.75	636	(0.63, 0.37)	[20]
2 (Ir)	200	n/a	2.02	642	(0.63, 0.37)	[20]
3 (Ir)	119	n/a	1.22	651	(0.64, 0.35)	[20]
1	808	110	0.73	618	(0.59, 0.36)	[a]
2	525	262	0.20	692	(0.56, 0.28)	[a]

[a] This work.

fabricating red-emitting devices with excellent thermal stability, and may find utility in display and lighting technologies.

Conflicts of interest

None.

Author contributions

The manuscript was written through contributions of all authors. All authors have given approval to the final version of the manuscript.

Acknowledgements

This work was supported by the Basic Science Research Program through the National Research Foundation of Korea (NRF), funded by the Ministry of Education, Science and Technology (NRF-2016R1D1A1B02013505) and the Brain Korea 21 Plus Project.

Appendix A. Supplementary data

Supplementary data related to this article can be found at http://dx.doi.org/10.1016/j.orgel.2017.12.035.

References

[1] Q. Pei, G. Yu, C. Zhang, Y. Yang, A.J. Heeger, Polymer light-emitting electrochemical cells, Science 269 (1995) 1086–1088.
[2] J.D. Slinker, A.A. Gorodetsky, M.S. Lowry, J. Wang, S. Parker, R. Rohl, S. Bernhard, G.G. Malliaras, Efficient yellow electroluminescence from a single layer of a cyclometalated iridium complex, J. Am. Chem. Soc. 126 (2004) 2763–2767.
[3] C.D. Sunesh, G. Mathai, Y. Choe, Constructive effects of long alkyl chains on the electroluminescent properties of cationic iridium complex-based light-emitting electrochemical cells, ACS Appl. Mater. Interfaces 6 (2014) 17416–17425.
[4] C.D. Sunesh, K. Shanmugasundaram, M.S. Subeesh, R.K. Chitumalla, J. Jang, Y. Choe, Blue and blue-green light-emitting cationic iridium complexes: synthesis, characterization, ACS Appl. Mater. Interfaces 7 (2015) 7741–7751.
[5] S.B. Meier, D. Tordera, A. Pertegás, C. Roldán-Carmona, E. Ortí, H.J. Bolink, Light-emitting electrochemical cells: recent progress and future prospects, Mater. Today 17 (2014) 217–223.
[6] R.D. Costa, E. Ortí, H.J. Bolink, S. Graber, C.E. Housecroft, E.C. Constable, Intramolecular π-stacking in a phenylpyrazole-based iridium complex and its use in light-emitting electrochemical cells, J. Am. Chem. Soc. 132 (2010) 5978–5980.
[7] R.D. Costa, E. Ortí, H.J. Bolink, F. Monti, G. Accorsi, N. Armaroli, Luminescent ionic transition-metal complexes for light-emitting electrochemical cells, Chem. Int. Ed. 51 (2012) 8178–8211.
[8] C.D. Sunesh, M. Chandran, G. Mathai, Y. Choe, Highly luminescent yellow and yellowish-green light-emitting electrochemical cells based on cationic iridium complexes with phenanthroline based ancillary ligands, Opt. Mater. 35 (2013) 407–413.
[9] C.D. Sunesh, G. Mathai, Y.-R. Cho, Y. Choe, Optoelectronic properties of green and yellow light-emitting electrochemical cells based on cationic iridium complexes, Polyhedron 57 (2013) 77–82.
[10] C.D. Sunesh, G. Mathai, Y. Choe, Green and blue–green light-emitting electrochemical cells based on cationic iridium complexes with 2-(4-ethyl-2-pyridyl)-1H-imidazole ancillary ligand, Org. Electron. 15 (2014) 667–674.
[11] H. Rudmann, M.F. Rubner, Single layer light-emitting devices with high efficiency and long lifetime based on tris(2,2' bipyridyl) ruthenium(II) hexafluorophosphate, J. Appl. Phys. 90 (2001) 4338–4345.
[12] H. Rudmann, S. Shimada, M.F. Rubner, Solid-state light-emitting devices based on the tris-chelated ruthenium(II) complex. 4. high-efficiency light-emitting devices based on derivatives of the tris(2,2'-bipyridyl) ruthenium(II) complex, J. Am. Chem. Soc. 124 (2002) 4918–4921.
[13] J.K. Lee, D.S. Yoo, E.S. Handy, M.F. Rubner, Thin film light emitting devices from an electroluminescent ruthenium complex, Appl. Phys. Lett. 69 (1996) 1686–1688.
[14] C.D. Sunesh, O. Sunseong, M. Chandran, D. Moon, Y. Choe, Effect of ionic liquids on the electroluminescence of yellowish-green light-emitting electrochemical cells using bis(2-(2,4-difluorophenyl)pyridine)4,7-diphenyl-1,10-phenanthroline-iridium(III) hexafluorophosphate, Mater. Chem. Phys. 136 (2012) 173–178.
[15] C.D. Sunesh, S. Ok, G. Mathai, Y. Choe, Electroluminescent properties of yellow light-emitting electrochemical cells based on a cationic iridium complex and the effect of ionic liquids incorporation in an active layer, Thin Solid Films 531 (2013) 530–534.
[16] C.D. Sunesh, Y. Choe, Synthesis and characterization of cationic iridium complexes for the fabrication of green and yellow light-emitting devices, Chem. Phys. 156 (2015) 206–213.
[17] D. Tordera, A. Pertegas, N.M. Shavaleev, R. Scopelliti, E. Orti, H.J. Bolink, E. Baranoff, M. Gratzel, M.K. Nazeeruddin, Efficient orange light-emitting electrochemical cells, J. Mater. Chem. 22 (2012) 19264–19268.
[18] H.C. Su, F.C. Fang, T.Y. Hwu, H.H. Hsieh, H.F. Chen, G.H. Lee, S.M. Peng, K.T. Wong, C.C. Wu, Highly efficient orange and green solid-state light-emitting electrochemical cells based on cationic Ir^{III} complexes with enhanced steric hindrance, Adv. Funct. Mater. 17 (2007) 1019–1027.
[19] J.E. Namanga, N. Gerlitzki, B. Mallick, A.-V. Mudring, Long term stable deep red light-emitting electrochemical cells based on an emissive, rigid cationic Ir(iii) complex, J. Mater. Chem. C 5 (2017) 3049–3055.
[20] C.D. Ertl, C. Momblona, A. Pertegás, J.M. Junquera-Hernández, M.-G. La-Placa, A. Prescimone, E. Ortí, C.E. Housecroft, E.C. Constable, H.J. Bolink, Highly stable red-light-emitting electrochemical cells, J. Am. Chem. Soc. 139 (2017) 3237–3248.
[21] A.K. Pal, D.B. Cordes, A.M.Z. Slawin, C. Momblona, A. Pertegas, E. Orti, H.J. Bolink, E. Zysman-Colman, Simple design to achieve red-to-near-infrared emissive cationic Ir(iii) emitters and their use in light emitting electrochemical cells, RSC Adv. 7 (2017) 31833–31837.
[22] L. Donato, C.E. McCusker, F.N. Castellano, E. Zysman-Colman, Mono- and dinuclear cationic iridium(III) complexes bearing a 2,5-dipyridylpyrazine (2,5-dpp) ligand, Inorg. Chem. 52 (2013) 8495–8504.
[23] J.L. Rodriguez-Redondo, R.D. Costa, E. Orti, A. Sastre-Santos, H.J. Bolink, F. Fernandez-Lazaro, Red-light-emitting electrochemical cell using a polypyridyl iridium(iii) polymer, Dalton Trans. (2009) 9787–9793.
[24] Y. Li, N. Dandu, R. Liu, Z. Li, S. Kilina, W. Sun, Effects of extended π-conjugation in phenanthroline (N∧N) and phenylpyridine (C∧N) ligands on the photophysics and reverse saturable absorption of cationic heteroleptic iridium(III) complexes, J. Phys. Chem. C 118 (2014) 6372–6384.
[25] X. Zhu, L. Lystrom, S. Kilina, W. Sun, Tuning the photophysics and reverse saturable absorption of heteroleptic cationic iridium(III) complexes via substituents on the 6,6′-bis(fluoren-2-yl)-2,2′-biquinoline ligand, Inorg. Chem. 55 (2016) 11908–11919.
[26] S. Graber, K. Doyle, M. Neuburger, C.E. Housecroft, E.C. Constable, R.D. Costa, E. Ortí, D. Repetto, H.J. Bolink, A supramolecularly-caged ionic iridium(III) complex yielding bright and very stable solid-state light-emitting electrochemical cells, J. Am. Chem. Soc. 130 (2008) 14944–14945.
[27] L. He, L. Duan, J. Qiao, G. Dong, L. Wang, Y. Qiu, Highly efficient blue-green and white light-emitting electrochemical cells based on a cationic iridium complex with a bulky side group, Chem. Mater. 22 (2010) 3535–3542.
[28] Y. Liu, M.S. Liu, A.K.Y. Jen, Synthesis and characterization of a novel and highly efficient light-emitting polymer, Acta Polym. 50 (1999) 105–108.
[29] S.-W. Hwang, Y. Chen, Synthesis and electrochemical and optical properties of novel poly(aryl ether)s with isolated carbazole and p-quaterphenyl chromophores, Macromolecules 34 (2001) 2981–2986.
[30] E.A. Steck, A.R. Day, Reactions of phenanthraquinone and retenequinone with aldehydes and ammonium acetate in acetic acid solution1, J. Am. Chem. Soc. 65 (1943) 452–456.
[31] S. Rosepriya, A. Thiruvalluvar, J. Jayabharathi, M. Venkatesh Perumal, R.J. Butcher, J.P. Jasinski, J.A. Golen, 1,2-Diphenyl-1H-imidazo[4,5-*f*][1,10]phenanthroline, o989–o989, Acta Crystallogr. Sect. E.-Struct Rep. Online 67 (2011).
[32] K. Skonieczny, A.I. Ciuciu, E.M. Nichols, V. Hugues, M. Blanchard-Desce, L. Flamigni, D.T. Gryko, Bright, Emission tunable fluorescent dyes based on imidazole and [small pi]-expanded imidazole, J. Mater. Chem. 22 (2012) 20649–20664.
[33] M.J. Frisch, G.W. Trucks, H.B. Schlegel, G.E. Scuseria, M.A. Robb, J.R. Cheeseman, G. Scalmani, V. Barone, B. Mennucci, G.A. Petersson, H. Nakatsuji, M. Caricato, X. Li, H.P. Hratchian, A.F. Izmaylov, J. Bloino, G. Zheng, J.L. Sonnenberg, M. Hada, M. Ehara, K. Toyota, R. Fukuda, J. Hasegawa, M. Ishida, T. Nakajima, Y. Honda,

O. Kitao, H. Nakai, T. Vreven, J.A. Montgomery, J.E. Peralta, F. Ogliaro, M. Bearpark, J.J. Heyd, E. Brothers, K.N. Kudin, V.N. Staroverov, R. Kobayashi, J. Normand, K. Raghavachari, A. Rendell, J.C. Burant, S.S. Iyengar, J. Tomasi, M. Cossi, N. Rega, J.M. Millam, M. Klene, J.E. Knox, J.B. Cross, V. Bakken, C. Adamo, J. Jaramillo, R. Gomperts, R.E. Stratmann, O. Yazyev, A.J. Austin, R. Cammi, C. Pomelli, J.W. Ochterski, R.L. Martin, K. Morokuma, V.G. Zakrzewski, G.A. Voth, P. Salvador, J.J. Dannenberg, S. Dapprich, A.D. Daniels, J.B. Farkas, J.V. Foresman, J. Ortiz, Cioslowski, D.J. Fox, Gaussian 09, Revision B.01, Wallingford CT (2009).

[34] A.D. Becke, Density-functional thermochemistry. III. the role of exact exchange, J. Chem. Phys. 98 (1993) 5648–5652.

[35] A.D. Becke, Density-functional thermochemistry. IV. A new dynamical correlation functional and implications for exact-exchange mixing, J. Chem. Phys. 104 (1996) 1040–1046.

[36] C. Lee, W. Yang, R.G. Parr, Development of the colle-salvetti correlation-energy formula into a functional of the electron density, Phys. Rev. B 37 (1988) 785–789.

[37] P.J. Hay, W.R. Wadt, Ab initio effective core potentials for molecular calculations. Potentials for the transition metal atoms Sc to Hg, J. Chem. Phys. 82 (1985) 270–283.

[38] P.J. Hay, W.R. Wadt, Ab initio effective core potentials for molecular calculations. potentials for K to Au including the outermost core orbitals, J. Chem. Phys. 82 (1985) 299–310.

[39] W.R. Wadt, P.J. Hay, Ab initio effective core potentials for molecular calculations. potentials for main group elements Na to Bi, J. Chem. Phys. 82 (1985) 284–298.

[40] S. Sprouse, K.A. King, P.J. Spellane, R.J. Watts, Photophysical effects of metal-carbon.sigma. bonds in ortho-metalated complexes of iridium(III) and rhodium(III), J. Am. Chem. Soc. 106 (1984) 6647–6653.

[41] S. Lamansky, P. Djurovich, D. Murphy, F. Abdel-Razzaq, H.-E. Lee, C. Adachi, P.E. Burrows, S.R. Forrest, M.E. Thompson, Highly phosphorescent bis-cyclometalated iridium complexes: synthesis, photophysical characterization, and use in organic light emitting diodes, J. Am. Chem. Soc. 123 (2001) 4304–4312.

[42] M.G. Colombo, T.C. Brunold, T. Riedener, H.U. Guedel, M. Fortsch, H.-B. Buergi, Facial tris cyclometalated rhodium(3+) and iridium(3+) complexes: their synthesis, structure, and optical spectroscopic properties, Inorg. Chem. 33 (1994) 545–550.

[43] A.B. Tamayo, S. Garon, T. Sajoto, P.I. Djurovich, I.M. Tsyba, R. Bau, M.E. Thompson, Cationic bis-cyclometalated iridium(III) diimine complexes and their use in efficient blue, green, and red electroluminescent devices, Inorg. Chem. 44 (2005) 8723–8732.

[44] T. Hu, L. Duan, J. Qiao, L. He, D. Zhang, R. Wang, L. Wang, Y. Qiu, Stable blue-green light-emitting electrochemical cells based on a cationic iridium complex with phenylpyrazole as the cyclometalated ligands, Inorg. Chem. 13 (2012) 1948–1955.

[45] M.S. Lowry, J.I. Goldsmith, J.D. Slinker, R. Rohl, R.A. Pascal, G.G. Malliaras, S. Bernhard, Single-layer electroluminescent devices and photoinduced hydrogen production from an ionic iridium(III) complex, Chem. Mater. 17 (2005) 5712–5719.

[46] L. He, L. Duan, J. Qiao, R. Wang, P. Wei, L. Wang, Y. Qiu, Blue-emitting cationic iridium complexes with 2-(1H-pyrazol-1-yl)pyridine as the ancillary ligand for efficient light-emitting electrochemical cells, Adv. Funct. Mater. 18 (2008) 2123–2131.

[47] W.-L. Jia, Y.-F. Hu, J. Gao, S. Wang, Linear and star-shaped polynuclear Ru(ii) complexes of 2-(2[prime or minute]-pyridyl)benzimidazolyl derivatives: syntheses, photophysical properties and red light-emitting devices, Dalton Trans. (2006) 1721–1728.

[48] P. Dreyse, B. Loeb, M. Soto-Arriaza, D. Tordera, E. Orti, J.J. Serrano-Perez, H.J. Bolink, Effect of free rotation in polypyridinic ligands of Ru(ii) complexes applied in light-emitting electrochemical cells, Dalton Trans. 42 (2013) 15502–15513.